Detection of 3′-End RNA Uridylation with a Protein Nanopore

Massimiliano Clamer,[†,‡] Lajos Höfler,[†] Ellina Mikhailova,[†] Gabriella Viero,[‡,§] and Hagan Bayley[†,*]

[†]Department of Chemistry, University of Oxford, 12 Mansfield Road, Oxford OX1 3TA, United Kingdom, [‡]Laboratory of Translational Genomics, Center for Integrative Biology, University of Trento, Via delle Regole, 101 38123 Mattarello (TN), Italy, and [§]Institute of Biophysics, CNR, Via alla Cascata 56/C, 38123 (Povo) Trento, Italy

ABSTRACT Post-transcriptional modifications of the 3′-ends of RNA molecules have a profound impact on their stability and processing in the cell. Uridylation, the addition of uridines to 3′-ends, has recently been found to be an important regulatory signal to stabilize the tagged molecules or to direct them toward degradation. Simple and cost-effective methods for the detection of this post-transcriptional modification are not yet available. Here, we demonstrate the selective and transient binding of 3′-uridylated ssRNAs inside the β barrel of the staphylococcal α-hemolysin (αHL) nanopore and investigate the molecular basis of uridine recognition by the pore. We show the discrimination of 3′-oligouridine tails on the basis of their lengths and propose the αHL nanopore as a useful sensor for this biologically relevant RNA modification.

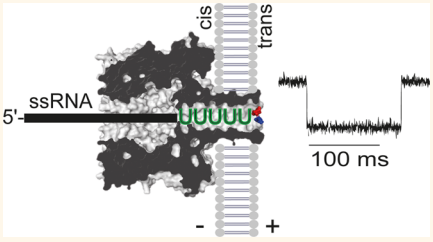

KEYWORDS: RNA · post-transcriptional modification · nanopore · α-hemolysin · RNA sensor · untranslated regions

RNA 3′-uridylation is a post-transcriptional modification that modulates gene expression.[1−3] The 3′-addition of a variable number (usually <20) of uridines plays a crucial role in determining the rate of mRNA degradation[4−6] and the turnover of microRNAs.[7−9] Today, the determination of oligo(U) tail abundance and length is still demanding. For this reason, the development of single-molecule techniques for the detection of this post-transcriptional modification is an attractive challenge.

α-Hemolysin (αHL) has been extensively used for the stochastic detection and analysis of a wide variety of molecules. Intensive studies on the interaction and translocation of nucleic acids through the αHL nanopore have allowed (*inter alia*) the analysis of single-stranded nucleic acid length[10] and DNA duplex dissociation and unzipping.[11,12] Nucleobase recognition with nanopores has been investigated after the immobilization of single strands within the pore[13−15] and by the identification of individual bases enzymatically cleaved from a longer DNA strand.[16] Short RNA or DNA sequence signatures can also be recognized by nanopores, by hybridization of complementary DNA probes to the target sequence,[17−19] or by using RNA-binding proteins that selectively bind a single-stranded RNA.[20] Despite these earlier studies, little work has been done on the direct single-molecule detection of specific RNA sequences.

In the present work, we used the αHL pore for the rapid, label-free, and stochastic detection of short 3′-uridylated RNAs, without the need for amplification. We demonstrated the selective binding of 3′-oligo(U) tails inside the β barrel of the αHL pore and investigated the molecular basis of uridine recognition.

RESULTS AND DISCUSSION

Selective RNA Sequence Detection. We explored the possibility that the αHL pore might recognize different nucleotides (G, C, U, A) at the 3′-end of ssRNA 10-mers. We added ssRNAs with sequence 5′-C_5X_5 (X = G, C, U, A) to the *cis* side of a lipid bilayer containing a single αHL pore (Figure 1a) in *low ionic strength buffer* (150 mM KCl, 100 mM NaCl, 2 mM $MgCl_2$, 10 mM HEPES, pH 6.5, in DMPC-treated water) (see Materials and Methods). We observed long current blockades (>5 ms) only when uridines were located at the 3′-end of the oligonucleotide (*i.e.*, X = U). Nucleotides others than uridine did not produce blockades (Figure 1b), suggesting that the αHL pore recognized the U_5 sequence. An A_5 tail produced fast spikes ($\bar{\tau}_D$ < 1 ms) in agreement with previously reported observations (Figure 1b).[21] For C_5U_5, the mean dwell time ($\bar{\tau}_D$) was 56 ± 7 ms

* Address correspondence to hagan.bayley@chem.ox.ac.uk.

Received for review September 27, 2013 and accepted December 26, 2013.

Published online December 26, 2013
10.1021/nn4050479

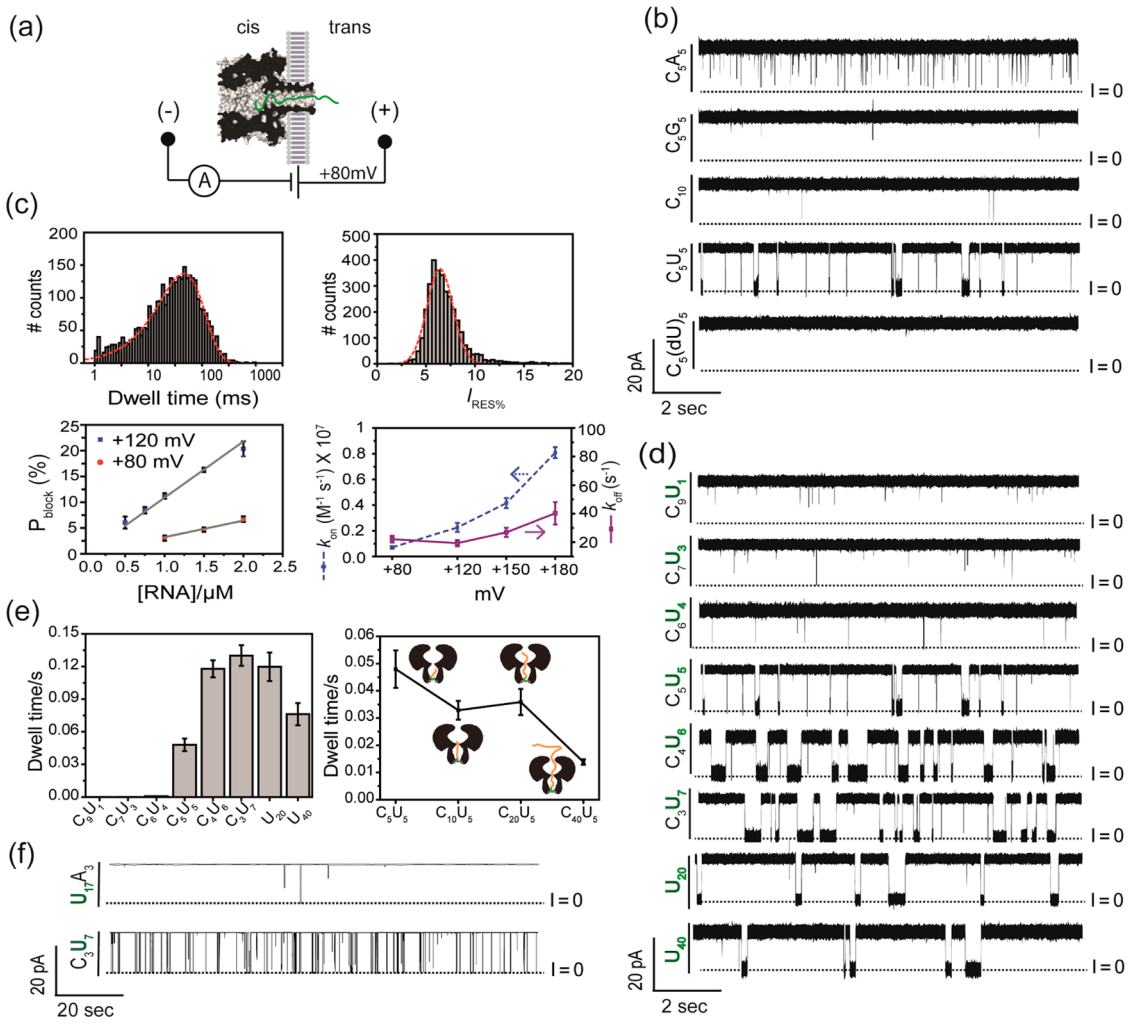

Figure 1. Nanopore detection of an oligouridine RNA sequence. (a) Cartoon showing the hypothetical RNA•nanopore interaction. The αHL nanopore (PDB: 7AHL) is embedded in a lipid bilayer. An RNA molecule (green line) is shown translocating from the *cis* to the *trans* side of the bilayer under a positive potential. (b) Single-channel ionic current recordings of the αHL nanopore in the presence of ssRNAs with different homopentameric 3′-extensions. Current traces were recorded at +80 mV in 150 mM KCl, 100 mM NaCl, 2 mM $MgCl_2$, 10 mM HEPES, pH 6.5 (low ionic strength buffer). The signal was filtered at 2 kHz and sampled at 20 kHz. (c) Top left: Distribution of C_5U_5 dwell times. A single-component probability density function was fitted (~3000 events). The mean dwell time ($\bar{\tau}_D$) for C_5U_5 was 52 ± 9 ms at +120 mV (n = 4) and 56 ± 7 ms at +80 mV (n = 16). Top right: Histogram of $I_{RES\%}$ for C_5U_5. The distribution was fitted to a Gaussian function, yielding the mean ± SD. The results in "c, top" are from a single experiment. Bottom left: RNA concentration dependence of the overall probability that the pore was occupied by RNA (P_{block}) at +80 mV (red points) and +120 mV (blue points) (n = 5). P_{block} was calculated from $\bar{\tau}_{on}$ and $\bar{\tau}_{off}$ values as described in Materials and Methods. Gray lines represent a fit to P_{block} for each concentration point (linear regression). Bottom right: Voltage dependences of the rate constants k_{on} (blue, broken line) and k_{off} (purple, solid line) for C_5U_5 (mean ± SD, n = 3). Arrows indicate the color-coded y-axis. (d) Ionic current traces for ssRNAs with different oligo(U) tail lengths. (e) Left: Mean dwell times ± SD for various ssRNAs. Right: Effect of the length of the non-U 5′-extensions on dwell times. (f) Effect of the position of the oligouridine sequence on the blockade events. Data were acquired as in "b". Traces were filtered with a digital filter at 20 Hz for display. I = 0, zero current level.

(mean ± SD, n = 16 experiments), with the majority of the events (>90%) longer than 5 ms (Figure 1c). No blockades were observed when C_5U_5 was added to the *trans* compartment under a negative potential (Supporting Information Figure SI1), suggesting that the interaction of C_5U_5 with the pore is orientation-specific. The residual current ($I_{RES\%}$; see Materials and Methods) during the ssRNA blockade indicated an almost complete block of the channel ($I_{RES\%}$ < 6 ± 1%, n = 5) (Figure 1c).

We next investigated whether the long blockades were RNA-selective. We placed deoxyridines (dU) at the 3′-end (*i.e.*, X = dU in 5′-C_5X_5, the cytidines are ribonucleotides), and we did not observe long blockades, demonstrating a preferential blocking by ribonucleotides with respect to deoxynucleotides.

To further characterize the ssRNA blocking, the concentration and voltage dependence of blockades were measured. The blockade frequency $1/\bar{\tau}_{on}$ (s^{-1}) was linearly proportional (R^2 = 0.96) to the concentration of the ssRNA (Figure SI2). The association rate costant, k_{on}, was derived from the linear fit to $1/\bar{\tau}_{on} = k_{on} \times$ [RNA]. This finding is consistent with a bimolecular interaction between RNA and the αHL pore.

In contrast, the dissociation rate $1/\bar{\tau}_{off}$ (s^{-1}) was independent of RNA concentration (Figure SI2), as a consequence of the overall probability that the pore was occupied by the ssRNA ($P_{block\%}$; see Materials and Methods) was linearly proportional to RNA concentration (Figure 1c, bottom left, $R^2 = 0.99$). The distributions of the dwell times and interevent intervals (all event histograms) were fitted to single-component probability density functions to obtain the association, k_{on} (M^{-1} s^{-1}), and dissociation, k_{off} (s^{-1}), rate constants. We found that both the k_{on} and the k_{off} for C_5U_5 (2 μM) increased with increasing voltage (Figure 1c, bottom right, and Figure SI3).

Previous studies of the translocation of homopolymeric RNA molecules (from ~100 to ~500 nt) through the αHL pore reported values of $\bar{\tau}_D$ much smaller (~1−22 μs per nucleobase)[21−23] than we observed. However, there are several important experimental differences between these studies: (i) the ssRNAs used here were shorter than those used in previous studies;[10,21] (ii) we employed synthetic oligonucleotides, rather than oligouridine fragments obtained from the alkaline hydrolysis of polyuridylic acid[10] (this means a different chemical structure of the 3′-end); and (iii) our single-channel measurements were performed in 150 mM KCl instead of in 1 M KCl.[21] We found exceptionally long events ($\bar{\tau}_D$ > 50 ms) with short oligonucleotides (10 nt) possessing 3′-oligo(U) tails, suggesting the hypothesis that these blockades were caused by specific binding of the oligouridine sequence to the αHL pore.

To test this hypothesis, we varied the length of the 3′-oligo(U) sequence. We found that both the length and the position of the U stretch determined the duration of the current blockade (Figure 1d,e). Single-stranded RNAs 10−40 bases long with 3′-tails of four or more uridines exhibited long binding events (Figure 1d). When the oligo(U) tail was instead placed at the 5′-end or in the middle of the RNA oligonucleotide (Figures 1f and SI4), the dwell times were significantly shorter. Moreover, the $\bar{\tau}_D$ of ssRNAs 10 nt long increased with the length of the 3′-oligo(U) tail (Figure 1e, left). Additionally, the $\bar{\tau}_D$ of both 5′-U_n and 5′-C_nU_5 decreased as the strand length increased ($n \geq 5$) (Figure 1e, right).

The alkaline fragmentation of polyuridylic acid[10] leaves a 2′,3′-cyclic monophosphate, which is further hydrolyzed to give a mixture of 2′- and 3′-monophosphates. We therefore explored the possibility that 3′-ribose phosphorylation affects the oligonucleotide binding affinity. Indeed, the $\bar{\tau}_D$ of 3′-phosphorylated C_3U_7 was >3-fold lower than nonphosphorylated C_3U_7 (30 ± 2 *versus* 114 ± 2 ms, n = 3) (Figure 2a,b).

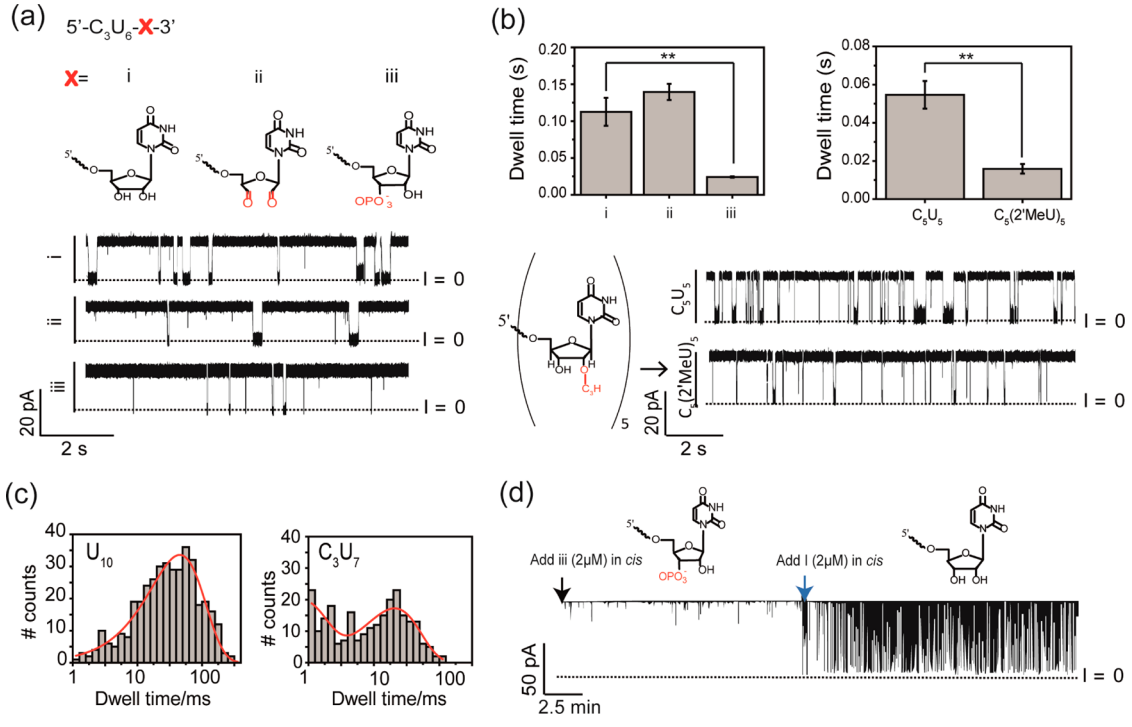

Figure 2. WT-αHL pore binds ssRNAs: effect of ionic strength and the 3′-terminal nucleotide. (a) Current blockades produced by ssRNA decamers with different 3′-sugar rings: (i) ribose with a free 3′-OH, (ii) the 2′,3′-dialdehyde, (iii) ribose with a 3′-phosphate. Recordings were performed in low ionic strength buffer at +80 mV (n = 3). (b) Histograms of mean dwell times for the three different RNAs in "a" (right) and for a ssRNA with five 2′-*O*-methyluridines [$C_5(MeU)_5$] at the 3′-end (left) (**) $P < 0.05$, Student's t-test. Bottom panel: Ionic current traces for C_5U_5 and $C_5(MeU)_5$ recorded at +80 mV in low ionic strength buffer. (c) Dwell time distributions in high ionic strength buffer (1 M KCl, 10 mM Tris HCl, 0.1 mM EDTA, pH 7.5 in DMPC water) for U_{10} (left) and C_3U_7 (right) (number of events >100). Recordings were made under an applied potential of +80 mV. (d) Current trace of αHL in the presence of 2 μM 3′-phosphorylated C_3U_7. Dephosphorylated C_3U_7 (2 μM) was added at the blue arrow. The signal was filtered at 2 kHz (low-pass Bessel filter) and sampled at 20 kHz. I = 0, zero current level.

To further explore the effect of the nucleotide chemistry at the 3′-end, we probed the RNA recognition within the nanopore using short (10 nt) oligonucleotides with substituted bases (Figure 2a,b). The substitution of a 3′-terminal uridine (*i.e.*, X = U) with cytosine (*i.e.*, X = C) in the oligonucleotide U_9X_1 reduced the dwell time ~3-fold (from 101 ± 9 to 27 ± 2 ms, $n = 3$). However, 3′-terminal substitution with deoxyuridine (*i.e.*, X = dU) did not significantly change the dwell time (Figure SI4a,b). Blockades were not seen when fewer than four uridines were placed at the 3′-end (Figure SI4c), suggesting that the last five 3′-ribonucleotides of the ssRNA are critical for inducing blockades.

The selective and complete oxidation of the 3′-terminal ribose to dialdehyde (Figure SI5) did not decrease the duration of the blockade ($\bar{\tau}_D$ = 140 ± 10 ms, $n = 3$, Figure 2a), but it did decrease the value of k_{on} (from (2.5 ± 0.2) × 10^6 to (0.5 ± 0.02) × 10^6 M^{-1} s^{-1}; n = 3, +120 mV) (Figure SI6). The presence of 2′-O-methylation on all five uridines in C_5U_5 caused a ~70% decrease in the duration of the blockade (16 ± 2 ms, n = 3) (Figure 2b). This difference can be interpreted in terms of a significant specificity of the docking events into a putative RNA binding site in the αHL pore.

In summary, 3′-uridylation of ssRNA can be detected by αHL as long current blockades if more than four uridines are present at the 3′-end and the chemistry of the 3′-end U tail (U > 4) can change the mean dwell time of the blockades.

Effect of Ionic Strength on RNA Binding. Previous studies of polymer translocation through protein pores have mostly been performed in high ionic strength (≥1 M KCl) buffers to increase current signal-to-noise.[13,24] However, ionic strength also modulates several properties of the ssRNA (*e.g.*, persistence length)[25,26] and the protein−RNA interactions (*e.g.*, through charge screening) and so may, in turn, affect the sensitivity of nanopore detection. We observed that in high ionic strength buffer (1 M KCl, 10 mM Tris HCl, 0.1 mM EDTA, pH 7.5, in DMPC-treated water) the $\bar{\tau}_D$ of the ssRNA was reduced by more than 60% (Figure 2c and Table 1).

In contrast to low ionic strength conditions (Figure 2a), the addition of the 3′-phosphorylated C_3U_7 in high ionic strength buffer did not produce any blocking events (Figure 2d). The addition of ssRNAs with identical sequence but with a free 3′-OH on the terminal ribose did produce blockades (Figure 2d). This result shows the combined effect of the 3′-phosphorylation state and the ionic strength upon the sensitivity of the pore. These results also explain why, in previous studies[10,21] on the oligouridine translocation through the αHL pore, the long RNA blockades were not observed.

TABLE 1. Effect of Salt Concentration on the Binding of ssRNAs Containing Oligouridine Sequences[a]

RNA	HS buffer $\bar{\tau}_D$ (ms)	LS buffer $\bar{\tau}_D$ (ms)
U_{20}	46 ± 6	120 ± 13
U_{10}	39 ± 5	101 ± 10
C_3U_7	19 ± 3	130 ± 9

[a] HS: high ionic strength buffer, 1 M KCl, 10 mM Tris HCl, 0.1 mM EDTA, pH 7.5 in DMPC water. LS: low ionic strength buffer, 150 mM KCl, 100 mM NaCl, 2 mM $MgCl_2$, 10 mM HEPES in DMPC water, pH 6.5. The signal was filtered at 2 kHz with a low-pass Bessel filter and sampled at 20 kHz; $n = 3$.

Nature of the RNA Binding Site. To identify the binding site for the 3′-U_n (n > 4) tails, mutagenesis was performed on αHL (Figure 3a). We produced two mutants in which the mutation sites were located at opposite ends along the β barrel, facing the *cis* compartment (NN-*cis*, E111N/K147N) or the *trans* compartment (NNA-*trans*, D127N/D128N/K131A). The NN-*cis* mutation neutralized charged residues at the pore constriction[27] and widened the internal entrance to the β barrel.[28] These modifications are known to result in a decreased voltage threshold for nucleic acid translocation.[28] An analysis of the β barrel region of WT-αHL (Glu-111 to Lys-147) with BindN,[29] software that predicts RNA-binding residues (http://bioinfo.ggc.org/bindn/), gave a high binding score for the region between Tyr-125 and Lys-131 (see Supporting Information). The NNA-*trans* mutations neutralize the highly charged *trans* loops of the αHL β barrel in the predicted binding region.

The NN-*cis* mutation had no effect on current blockades elicited by C_3U_7. NNA-*trans* exhibited no long blockades with C_3U_7, although very short blockades ($\bar{\tau}_D$ < 1 ms) were observed (Figure 3b). We conclude that (i) the current blockades are not due to secondary structure of the RNA occluding the pore at the constriction;[30] and (ii) removing the charges at Asp-127, Asp-128, and Lys-131 prevents blockades by C_3U_7, suggesting the existence of an RNA binding site formed by these residues.

We then investigated the contributions of each of the three mutated positions in NNA-*trans* toward the binding of C_3U_7. We generated single- and double-point mutants, neutralizing the charges at positions 127, 128, and 131 (Figure SI7), and examined the effects of these mutations on the binding of C_3U_7, which binds tightly to the WT-αHL pore. Only D128N retained binding (Figure 3c). We hence conclude that Asp-128 does not participate in uridine recognition (Figures 3c and SI7). In fact, D128N has a significantly higher affinity than the WT-αHL pore ($K_D^{(D128N)}$ = 2.0 ± 0.9 μM; $K_D^{(WT)}$ = 11.6 ± 0.6 μM at +80 mV, n = 5; and $K_D^{(D128N)}$ = 1.3 ± 0.1 μM; $K_D^{(WT)}$ = 4.7 ± 0.8 μM at + 120 mV, n = 5).

On the basis of these findings, we speculated how Asp-127 and Lys-131 could be involved in the recognition of the RNA and how Asp-128 could affect those residues. Asp-128 can form salt bridges with Lys-131 on the neighboring subunit. Moreover, Asp-128 may perturb the pK_a of Asp-127, thereby reducing Coulomb

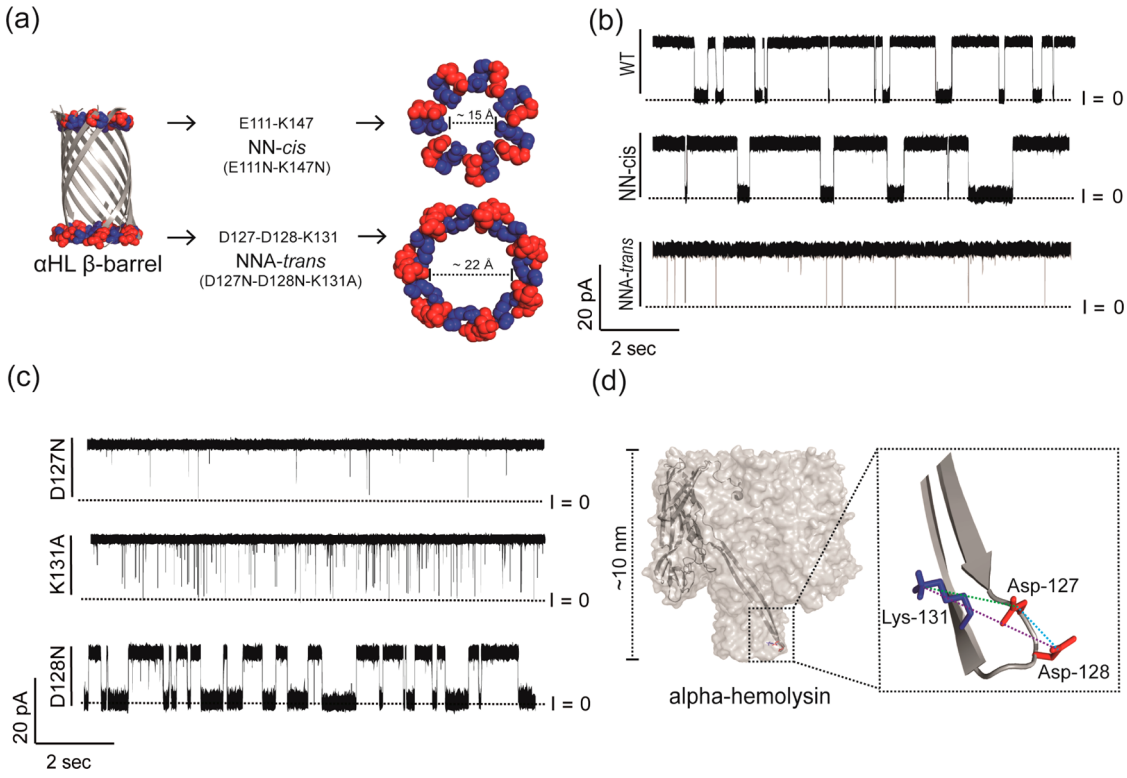

Figure 3. WT-αHL contains a ssRNA binding site. (a) Position of amino acid mutations in the β barrel of the WT-αHL pore. The constriction formed by the rings of residues Glu-111 and Lys-147 were mutated to Asn-111 and Asn-147 in the NN-*cis* mutant. The residues Asp-127, Asp-128, and Lys-131 were mutated to Asn-127, Asn-128, and Ala-131 in the NNA-*trans* mutant. The diameters of the two entrances of the WT-αHL β barrel are given. (b) Current traces showing 2 μM C_3U_7 detected by the WT-αHL pore (top), NN-*cis* (middle), and NN-*trans* (bottom), monitored at +80 mV in low ionic strength buffer. The signal was filtered at 2 kHz and acquired at 20 kHz. (c) Current traces of αHL pores formed from subunits with single-point mutations showing blockades by 2 μM C_3U_7 (*cis*) at +80 mV in low ionic strength buffer. The signal was acquired as in "b". (d) Heptameric αHL pore with one of the seven subunits shown as a ribbon structure (dark gray). Zoom in: *trans* loop showing the three residues mutated in NNA-*trans*. The distance between Asp-127 and Lys-131 (from the C atom of the Asp carboxyl group to the N atom of the Lys amino side chain) is ~7.6 Å (green). Between Asp-128 and Lys-131, the distance is ~12.7 Å (violet), and between Asp-127 and Asp-128 (from carboxyl C atom to carboxyl C atom), it is ~5.2 Å (blue). From Lys-131 to the Asp-127 on the neighboring subunit, the distance is ~3.2 Å (not shown), and between Lys-131 and the Asp-128 on the neighboring subunit, the distance is ~3.7 Å (not shown).

interactions. In fact, the short distance between the carboxyl groups of Asp-128 and Asp-127 allows a possible interaction of the two side chains located on the same protein subunit. The distance between the C atom of the carboxyl group and the N atom of the amino group on the side chains of Asp-127 and Lys-131 of the same subunit is sufficient to allow the interaction (*e.g.*, cation−π interaction or hydrogen bonds) of the two functional groups with a uridine nucleotide residing between them (Figure 3d). It would be interesting to investigate similarities with RNA binding proteins that bind 3′-oligouridine tails, such as the family of Sm and Sm-like proteins.[31−35]

Overall, our experimental results suggest that the αHL pore is an ssRNA-binding nanopore with a strong affinity for 3′-end oligouridylated ssRNAs.

Number of Subunits Required for ssRNA Binding. We determined whether all seven monomers in the heptameric pore were simultaneously involved in binding oligo(U). Monomers of WT-αHL bearing a C-terminal D_8H_6 tail were used to aid the separation of heteroheptameric αHL pores by gel-shift electrophoresis.[36,37] The $\bar{\tau}_D$ values of αHL heteroheptamers revealed three populations of blockades, corresponding to strong binding ($\bar{\tau}_D \geq 100$ ms), weaker binding (5 ms $\leq \bar{\tau}_D \leq$ 100 ms), and no binding ($\bar{\tau}_D <$ 5 ms). Strong binding was observed only with the heteroheptamer containing a single mutated subunit. Weaker binding was found with heteroheptamers containing two to four NNA-*trans* subunits and no binding when more than four NNA-*trans* subunits were present (Figure SI8).

We conclude that the αHL nanopore binds RNA strands in a sequence-specific fashion with more than one protein subunit interacting with the ssRNA at once.

Proof of RNA Translocation. Although ssDNA and ssRNA translocation through the αHL pore has been previously demonstrated,[10,38] we could not dismiss the possibility that the short ssRNAs we examined visited the β barrel to produce a blockade but exited on the side of addition.

To demonstrate that the long current blockades arose from the translocation of ssRNA, a

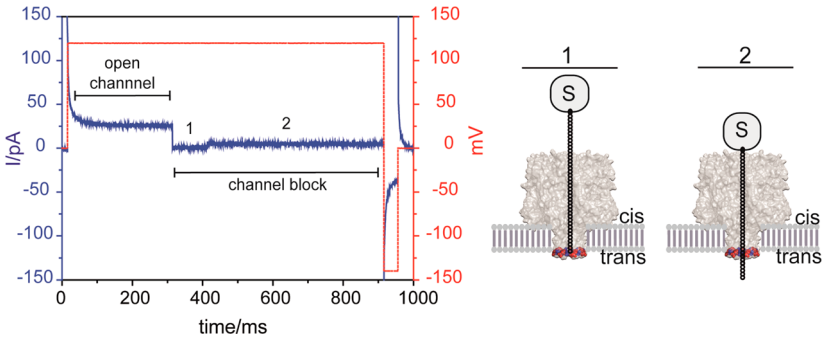

Figure 4. RNA current blockades are followed by translocation of the RNA through the αHL pore. Left: A biotinylated RNA•streptavidin complex (see the text) was added to the *cis* compartment at 2 μM and detected by the WT-αHL pore in low ionic strength buffer. An example of a single sweep is shown (blue, ionic current), resulting from an automated voltage protocol (red line): (i) 10 ms at 0 mV; (ii) 900 ms at +120 mV; (iii) 45 ms at −120 mV; (iv) 45 ms at 0 mV. The signal was filtered with a 2 kHz low-pass filter and acquired at 20 kHz. The protocol was repeated 1000 times in each experiment. The two levels associated with a blockade are labeled 1 and 2. Right: Schematic representations of the states associated with the two current levels: 1. RNA association with the binding site near the *trans* entrance (colored, space filling); 2. "permanent" block after translocation of the RNA•streptavidin complex.

streptavidin•(5′)biotin−RNA complex was formed[15] from a ssRNA 40-mer. With this complex, ~90% of the events were "permanent" blockades ($I_{RES\%} = 5.60 \pm 0.01$, $n = 3$) and required inversion of the voltage polarity to unblock the pore (Figures 4 and SI9).

Around 20% of the "permanent" blockades exhibited a two-step signal, where step 1 likely arose from the binding of the 3′-end of the ssRNA within the αHL pore. In fact, this step showed the same characteristics described above for oligo(U) interaction (low residual current and a long dwell time). Step 2 was a permanent current blockade that depended on the streptavidin attachment (Figures 4 and SI9). The increase in residual current of step 2, as compared to step 1, is probably due to the stretching of the RNA under the influence of the electric field.[15,39] Step 1 was not observed when we performed the same experiment with the homoheptameric αHL pore formed from D127N−K131A, which was incapable of RNA binding (Figure SI10). We believe that these data suggest that the ssRNA has passed through the pore in step 2 (Figure 4).

Moreover, it is unlikely that the ssRNA will return to the *cis* chamber given the strong electrophoretic force that acts on it and the resistance presented by the constriction at Glu-111 and Lys-147. Therefore, an RNA is not detected twice, which is a desirable feature for a single-molecule sensor.

αHL Pore as a Detector of 3′-End Uridylation. Next, we determined whether the WT-αHL pore could distinguish the number of uridines in 3′ using mixtures of ssRNAs with different length of the 3′-oligo(U) tails. Uridylated oligonucleotides tested in low ionic strength buffer showed different $\bar{\tau}_D$ values but similar $I_{RES\%}$ values. The $I_{RES\%}$ values were all <10%, and the small currents could not be distinguished. However, in high ionic strength buffer, we found that a mixture of four 10-mer RNAs with 3′-ends bearing 5, 6, 7, or 10 uridines could be discriminated by their mean $I_{RES\%}$ values (Figure 5a, Figure SI11, and Table 2). Interestingly, in these conditions, the RNAs also showed different mean dwell times (Table 2 and Figure SI12). Oligonucleotides with more than 10 bases caused a drop of the residual current to <10% (*e.g.*, $I_{\%RES}^{U20} = +7 \pm 1\%$), and the longer oligonucleotides could no longer be distinguished by their $I_{RES\%}$ values. Interestingly, with U_{20}, a second small population of events at higher residual current was observed (Figure 5a, bottom).

These results demonstrate that the WT-αHL pore can be used to distinguish the length of the 3′-U tail (U_n, $n \geq 5$) on short unstructured ssRNAs by using the mean residual currents and the mean dwell times.

Although the identification of long (≥5 uridines) homopolymeric tails could be useful for the biological characterization of 3′-end uridylations, the known biological relevance of short (<5 uridines) 3′-oligo(U) prompted us to improve the analysis. In fact, recently, it has been reported that mRNAs can be modified by poly(U) polymerases (PUP) such as Cid1. Cid1 adds uridines (usually <5 bases) to the 3′-end of mature polyadenylated mRNA in a poly(A)-independent manner.[40,41] Given these findings, we tested whether the D128N-αHL mutant pore could recognize U tails shorter than 5 bases in a fixed background of 15 adenosines.

First, we reasoned that, under our conditions, secondary structure in the ssRNA $A_{15}U_X$ ($X \leq 5$) would be energetically unfavorable (see Supporting Informations), so that blockades would not arise from unzipping of RNA duplexes. Then, we determined whether the background sequence of purines or pyrimidines affected the residence time of an oligo(U) sequence in the β barrel (Figure SI13). The dwell times of the blockades (Table 3) were directly correlated with the U tail length and not affected by the 5′-sequence. Finally, we demonstrated that the D128N-αHL pore was able to distinguish $A_{15}U_X$ ($X \leq 5$) ssRNAs based on $\bar{\tau}_D$ values in low ionic strength buffer (Figure 5b).

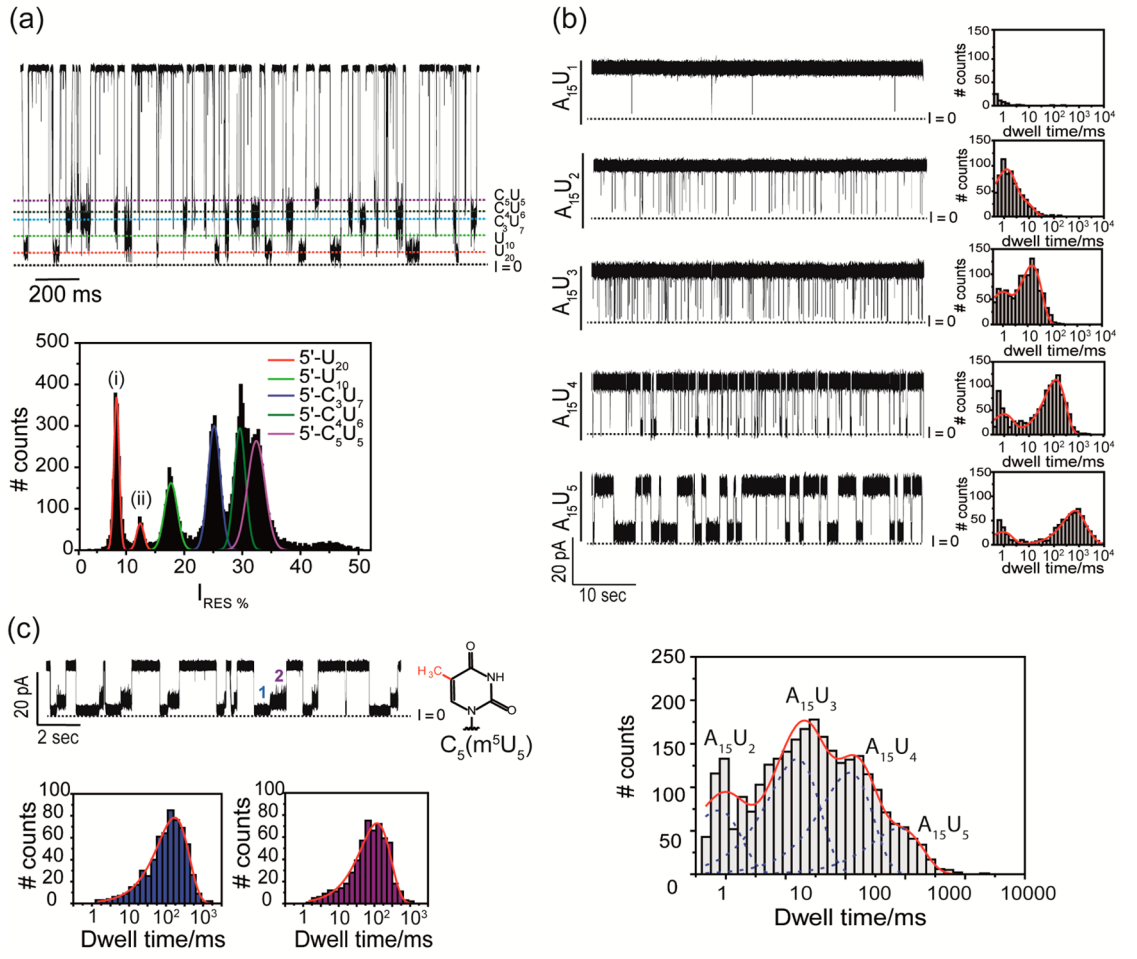

Figure 5. The αHL pore can detect different extents of RNA uridylation. (a) Top: Ion current trace in the presence of a mixture of C_5U_5, C_4U_6, C_3U_7, U_{10}, and U_{20} (all 2 μM). Dashed lines indicate the blockade levels associated with each ssRNA in high ionic strength buffer at +120 mV. The signal was filtered at 2 kHz and acquired at 20 kHz. Bottom: All-points histogram showing the distribution of $I_{RES\%}$ values (Table 2) for the ssRNAs used in "a". The data are fitted to Gaussian functions. U_{20} (red Gaussians) contributes a second small population of events at higher residual current (indicated by "ii") close to the main population (indicated by "i"). Open current level = 130 ± 5 pA. (b) Top: Current traces for the D128N pore in the presence of 2 μM ssRNA $A_{15}U_n$ ($1 \leq n \geq 5$) in the *cis* compartment (low ionic strength buffer, +120 mV, signal acquired as in "a"). On the right of each trace, the dwell time distribution for a typical 15 min trace is shown. Each histogram was fitted to a two-component probability density function. Bottom: Dwell time histogram for a mixture of ssRNAs ($A_{15}U_1$, $A_{15}U_2$, $A_{15}U_3$, $A_{15}U_4$, $A_{15}U_5$, 1 μM each, *cis*). $A_{15}U_1$ cannot be detected. The events can be fitted with a four-component probability density function (red line), which can be decomposed into single-component probability density functions (blue broken lines). Data were recorded in low ionic strength buffer at +120 mV. (c) Current trace for $C_5(m^5U)_5$. Two blockade levels (1 and 2) were observed for each translocation event in low ionic strength buffer (+80 mV). Level 2 always followed level 1. Bottom panels: Dwell time distributions for each level were fitted to single-component probability density functions (red lines). Signal acquired as in "a". *I* = 0, zero current level in all panels.

TABLE 2. Mean Dwell Times ($\bar{\tau}_D$) and Residual Currents ($I_{RES\%}$) for Various ssRNAs Detected by the WT-αHL Pore[a]

RNA	$\bar{\tau}_D$ (ms)^{HS}	$I_{RES\%}{}^{HS}$
U_{20}	46 ± 6	7 ± 1
U_{10}	39 ± 5	16 ± 1
C_3U_7	19 ± 3	24 ± 1
C_4U_6	10 ± 1	29 ± 1
C_5U_5	4.7 ± 0.3	32 ± 2

[a] Open current level = 130 ± 5 pA (mean ± SD, n = 3). Applied potential = +120 mV. HS: high ionic strength buffer. The signal was filtered at 2 kHz and acquired at 20 kHz (n = 3).

TABLE 3. Mean Dwell Times ($\bar{\tau}_D$) and Residual Currents ($I_{RES\%}$) for Various RNA Oligos Detected by the D128N-αHL Pore[a]

RNA	$\bar{\tau}_D$(ms)^{LS}	$I_{RES\%}{}^{LS}$	$\bar{\tau}_D$ (ms)^{HS}	$I_{RES\%}{}^{HS}$
$A_{15}U_2$	1.1 ± 0.2	1.5 ± 0.2	<1	13 ± 2
$A_{15}U_3$	15.2 ± 0.3	1.5 ± 0.2	3.4 ± 0.7	13 ± 2
$A_{15}U_4$	116 ± 8	1.5 ± 0.2	75 ± 4	13 ± 2
$A_{15}U_5$	820 ± 80	1.5 ± 0.2	148 ± 10	13 ± 2

[a] The signal was filtered at 2 kHz and acquired at 20 kHz. HS: high ionic strength buffer. LS: low ionic strength buffer. Open current level in LS, I_0 = 24 ± 2 pA (mean ± SD, n = 3); open current level in HS, I_0 = 130 ± 5 pA (mean ± SD, n = 3). Applied potential = +120 mV.

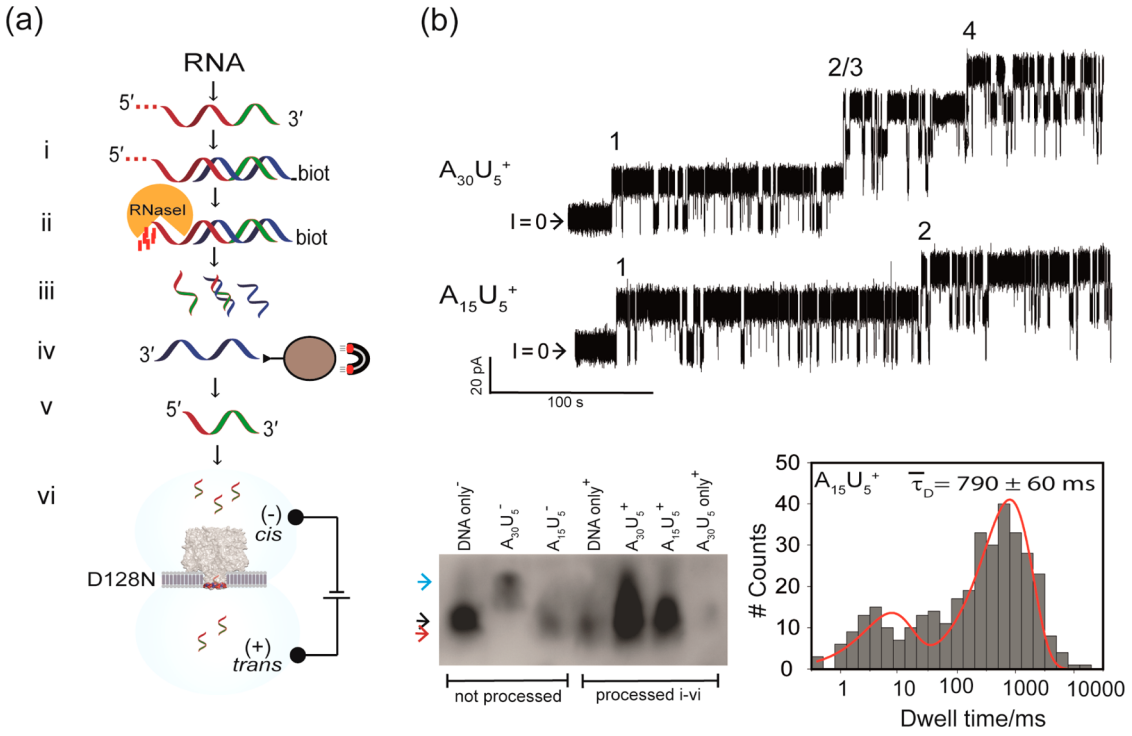

Figure 6. Protocol for RNA enrichment and uridylation analysis. (a) Protocol steps. (i) Annealing of model target RNA, $A_{30}U_5$ or $A_{15}U_5$, with the 5′-biotinylated DNA probe $A_{20}T_{15}$; (ii) digestion of the 5′ overhanging ssRNA with RNaseI; (iii) purification of the 3′-terminal fragment with a miRNAeasy column; (iv) removal of the DNA probe with streptavidin-conjugated magnetic beads; (v) DNase treatment; (vi) RNA fragments analyzed in DIBs with the D128N-αHL pore. (b) Top: current traces showing RNA blockades ($A_{30}U_5^+$ top, $A_{15}U_5^+$ bottom; processed as in "a"). Each single D128N pore in the bilayer showed RNA-binding activity (the number of inserted pores is marked). *I* = 0, zero current level. Bottom (left): 6 M urea polyacrylamide gel displaying the RNAs and DNA used in this experiment. (+) processed as in "a"; (−) control, not processed. Bottom (right): all data dwell time histogram of the blockades observed with $A_{15}U_5^+$. Traces were recorded in low ionic strength buffer. The signal was filtered at 1 kHz and acquired at 5 kHz.

We then asked whether the D128N-αHL pore was able to distinguish different 3′-U tail lengths in a mixture of $A_{15}U_1$, $A_{15}U_2$, $A_{15}U_3$, $A_{15}U_4$, and $A_{15}U_5$. The event durations were fitted to a four-component probability density function (Figure 5b, bottom panel). We found that the $\bar{\tau}_D$ values obtained from the mixture were the same as those found for the individual ssRNA (Table 3).

For all the oligonucleotides, a second population of shorter blockades (~1−5 ms) was recorded (Figure 5b). $A_{15}U_2$ gave only the shorter events, with a mean dwell time of 1.1 ± 0.1 ms (n = 3). The fact that $A_{15}U_1$ cannot be detected means that any RNAs without U or with only one U at the 3′-end are not identified by the pore. Therefore, we can argue that the presence of such molecules in a mixture does not affect the dwell time distribution of the events. Since we observed one molecule at time, undetected molecules or molecules outside the pores do not affect the dwell time distribution of the blockades.

These experiments demonstrated that the D128N-αHL pore can detect poly(A)$_{15}$ with more than one uridine at the 3′-end, and that it can distinguish the U lengths in a mixture of ssRNAs with more than two terminal uridines. In a typical experiment, we obtained between 200 and 400 events for each RNA population. We can use the mean dwell times determined from hundreds of events to identify sample species.

In high ionic strength buffer, the differences between the mean dwell times for $A_{15}U_2$, $A_{15}U_3$, $A_{15}U_4$, and $A_{15}U_5$ were smaller (Table 3 and Figure SI14), meaning that the high ionic strength condition affects RNA binding to the D128N pore, as it did for the WT-αHL pore. The identification of the RNA species by D128N-αHL is not possible using the mean residual current (Figure SI14).

In summary, the discrimination of longer (>10 nt) ssRNAs (here poly(A)$_{15}$) with short U tails can be achieved with the D128N-αHL mutant, in a low ionic strength buffer, by comparison of the mean dwell times.

Detection of RNA Methylation. In addition to the recognition of the extent of uridylation, the αHL pore could be used for the detection of ssRNAs containing non-canonical nucleobases. More than 100 nucleoside structural variations have been discovered recently.[42] For example, the methylation of uridine in the form of 5-methyluridine (m^5U) is a common modification in all the three domains of life and mainly affect tRNAs and rRNAs.[42]

We compared C_5U_5 with $C_5(m^5U)_5$ and observed blockades with a distinctive double current level for

the methylated oligonucleotide (called step 1 and step 2, Figure 5c). The steps had mean dwell times of $\bar{\tau}_{D1}$ = 143 ± 7 ms (n = 5) and $\bar{\tau}_{D2}$ = 56 ± 3 ms (n = 5). The total residence time ($\bar{\tau}_{D1} + \bar{\tau}_{D2}$) was remarkably longer than that of the control C_5U_5 ($\bar{\tau}_D$ = 56 ± 7 ms, n = 16, at +80 mV). Thus, the αHL nanopore can discriminate between strands incorporating normal uridine and methylated uridine.

Purification of Defined RNA Signature Fragments. The αHL pore can be used to detect oligouridine tails only on relatively short and unstructured ssRNAs. To test a practicable solution for sensing 3′-oligo(U) signatures of biological RNA samples, we developed a protocol for the enrichment of 3′-oligo(U) fragments from longer RNAs (Figure 6; see Supporting Information for details).

We optimized the protocol by using two synthetic RNAs ($A_{15}U_5$, $A_{30}U_5$). Briefly, (i) each ssRNA was independently annealed with a 5′-biotinylated DNA probe $A_{20}T_{15}$; (ii) the 5′ overhanging ssRNA was digested with RNaseI and the RNA/DNA mixture purified with miRNAeasy columns; (iii) the DNA probe was then separated by using streptavidin-coated magnetic beads; and (iv) the remaining solution was treated with DNase to remove residual DNA. Finally, (v) the purified RNA fragments were analyzed with the D128N-αHL pore by using droplet interface bilayers DIBs (see Materials and Methods). DIBs were used to ensure a high final RNA concentration (~1 μM, droplet volume <200 nL). Comparing the absorbance at 260 nm before and after application of the protocol to $A_{15}U_5$, the RNA recovery was found to be ~40%.

Blockades induced by the purified RNA fragments (from $A_{30}U_5$ and $A_{15}U_5$) showed the characteristic long dwell time distribution (>100 ms) seen previously (section "αHL Pore as a Detector of 3′-End Uridylation") in single-channel planar lipid bilayer recordings (PLM) for $A_{15}U_5$ with the D128N pore. The mean dwell time of the long blockades measured in DIBs for the processed $A_{30}U_5$ has been confirmed in PLM (Figures 6b and SI15). Residual DNA probe remained in the sample (Figure 6b), but it did not affect the signal (Figures SI15 and SI16). With this experiment, we demonstrated that the αHL pore can be employed as a sensor for uridylation with RNA obtained after digestion of the 5′-extension and purification of the remaining 3′-oligo-(U)-containing fragments.

Although we purified RNA fragments containing 3′-oligo(U), further improvements are needed in order to directly analyze the RNA obtained from biological samples. The complexity of a natural RNA cocktail will need supplementary pretreatments of the RNA sample, such as chemical coupling of the 3′-end with a functional probe to allow a specific fragmentation and to obtain RNA fragments suitable for our protocol.

CONCLUSIONS

Following the surprising observation of the affinity of the WT-αHL pore for oligo(U), we characterized the RNA•protein interaction by determining (1) the numbers of protein monomers required for the pore•RNA interaction, (2) the structural features of the RNA important for binding, (3) the amino acid residues of the pore involved in RNA binding, and (4) the rate constants for the interaction.

We found that 3′-end uridylated RNAs give distinctive blockades of the electrical current. Second, the $\bar{\tau}_D$ of the blockades is sensitive to the ionic strength of the buffer. Third, the αHL pore can discriminate both U tails of different length and the presence of noncanonical m^5U nucleobases. Fourth, our results demonstrate that the residues lining the lumen of αHL oligomers selectively interact with ssRNAs. Because more than one αHL subunit binds simultaneously to the oligo(U) sequence, a ssRNA cannot pass through the β barrel in a stretched conformation. Rather, a coiled RNA inside the β barrel most probably interacts with Asp-127 and Lys-131 residues across up to six of the seven subunits. Finally, our findings underline the importance of the 2′-hydroxyl group on the ribose for nucleic acid translocation through the pore.

In conclusion, the αHL nanopore is a fast, simple, and reliable stochastic sensor for post-transcriptional 3′-end uridylation and uracil methylation (m^5U) and may become an interesting tool for the characterization of biologically important RNA signatures.

MATERIALS AND METHODS

Planar Bilayer Recordings. As described in detail previously,[43] a 1,2-diphytanoyl-*sn*-glycero-3-phosphocholine (DPhPC, Avanti Polar Lipids) bilayer (~100 μm diameter) was created between the two compartments (each 1 mL) of a bilayer recording chamber. Experiments were performed under symmetrical buffer conditions. We used two buffers: low ionic strength buffer (150 mM KCl, 100 mM NaCl, 2 mM $MgCl_2$ and 10 mM HEPES at pH 6.5 titrated with NaOH) or high ionic strength buffer (1 M KCl, 10 mM Tris·HCl, 0.1 mM EDTA, pH 7.5). Solutions were made by using water (18.2 MΩcm, Millipore) treated with 0.1% v/v DMPC (dimethylpropyl carbonate) overnight at room temperature and then autoclaved to hydrolyze residual DMPC. Preformed αHL heptamers were added to the grounded *cis* compartment. Voltage was applied through a pair of Ag/AgCl electrodes set in salt bridges containing 3 M NaCl and 3% agar. After the insertion of a single αHL pore, the buffer was repeatedly replaced by manual pipetting to prevent multiple insertions. ssRNAs were introduced into the *cis* compartment and, after stirring, incubated in the electrolyte solution for ~5 min prior to data recording. The current was amplified by using a patch-clamp amplifier (Axopatch 200B, Axon Instruments), filtered with a low-pass Bessel filter (80 dB/decade) with a corner frequency of 2 kHz, and then digitized with a Digidata 1320 A/D converter (Axon Instruments) at a sampling frequency of 20 kHz for PLM experiments and 5 kHz for DIB experiments. The signal was not filtered further unless otherwise stated. The acquisition

software was Clampex 10.2 (Molecular Devices). The measurements were conducted at 20 ± 2 °C.

Data Analysis. Data analysis was performed with a custom python script using scipy, cython, and neo libraries.[44−46] The analysis was based on threshold searches. For the calculation of kinetic values, the traces were divided into open and blocked levels. The threshold level was chosen to be between the open and blocked levels. The transition between open and blocked levels was confirmed if both the rolling median of the last 100 data points and the last current value crossed the threshold level. The histograms of the logarithms of event times were fitted to a probability density functions (Pdf, eq 1), with single or multiple components:

$$\text{Pdf norm} = \sum_{j=1}^{n}\left(\frac{1}{\bar{\tau}_{D,j}}\cdot\exp\left[t_i - \frac{1}{\bar{\tau}_{D,j}}\cdot\exp(t_i)\right]\right) \quad (1)$$

where Pdf norm is the normalized frequency of event times, $\bar{\tau}_{D,j}$ is the mean dwell time or mean interevent interval for each distribution, and t_i is the duration of individual events. The rate constants k_{on} (M^{-1} s^{-1}) and k_{off} (s^{-1}) describing the current blockades were used to calculate the probability that the channel was blocked at any given moment ($P_{block\%}$):

$$P_{block}(\%) = \left\{1 - \left[\frac{\bar{\tau}_{on}}{\bar{\tau}_{on} + \bar{\tau}_{off}}\right]\right\} \times 100 \quad (2)$$

where $\bar{\tau}_{on}$ is the mean interevent interval and $\bar{\tau}_{off}$ is the mean dwell time.

Because the signature events for RNAs with oligo(U) tails (∼1−100 ms/nt) were well separated in duration from normal oligonucleotide translocations (∼1−20 μs/nt),[10] we set 1 ms as a cutoff for the rate constants analysis, unless otherwise stated. We included a binding event only when it was longer than 5 ms. In high ionic strength buffer and with the D128N mutant, a population of shorter events was recorded. Kinetic constants were calculated from the population of longer events.

The residual current ($I_{RES\%}$) of the RNA blockades as a percentage of I_O is given by

$$I_{RES\%} = \frac{I_b}{I_O} \times 100 \quad (3)$$

where I_O is the open pore current and I_b is the current through a pore partially blocked by RNA.

Data are presented as the mean ± SD of at least three independent experiments, and differences are considered statistically significant at $P < 0.05$ using the Student's t test.

DIBs. DPhPC lipids were purchased from Avanti Polar Lipids and dissolved in pentane at 5 mg mL^{-1}. A portion of the stock solution was evaporated by using a nitrogen stream followed by at least 30 min under vacuum. The residue was dissolved in a 1:1 (v/v) mixture of silicone oil (silicone oil AR 20) and hexadecane (both from Sigma-Aldrich). A droplet was formed by pipetting 200 nL of low ionic strength buffer supplemented with αHL heptamers and RNA (∼1 μM). Protein and RNA were in the droplet on the tip of the grounded electrode (*cis*). Another 200 nL droplet of buffer was added to the tip of the *trans* electrode. After bilayer formation, the *cis* electrode was moved away from the *trans* droplet until the bilayer diameter was approximately 150 μm, as monitored by capacitance measurement with a triangular voltage wave. The current signal was filtered at 1 kHz and acquired at 5 kHz, under an applied potential of +120 mV. Experiments were conducted at 20 ± 2 °C.

Conflict of Interest: The authors declare no competing financial interest.

Acknowledgment. This work was supported by grants from the National Institutes of Health and Oxford Nanopore Technologies. H.B. is the Founder, a Director, and a share-holder of Oxford Nanopore Technologies, a company engaged in the development of nanopore sequencing technology. Work in the Bayley laboratory at the University of Oxford, including this work, is supported in part by Oxford Nanopore Technologies. We thank Dr. R. Gomez, Dr. J. Cracknell, and L. Lercher for helpful comments. M.C. was supported by the Dematté studentship grant for international training.

Supporting Information Available: Details of experimental procedures, oligonucleotide sequences, and additional figures as described in the text (SI1−SI16) are available. This material is available free of charge *via* the Internet at http://pubs.acs.org.

REFERENCES AND NOTES

1. Song, M.; Kiledjian, M. 3′ Terminal Oligo U-Tract-Mediated Stimulation of Decapping. *RNA* **2007**, *13*, 2356–2365.
2. Choi, Y. S. U. N. S.; Patena, W.; Leavitt, A. D.; McManus, M. T. Widespread RNA 3′-End Oligouridylation in Mammals. *RNA* **2012**, *18*, 394–401.
3. Rissland, O.; Norbury, C. 3′ Uridylation Precedes Decapping in a Novel Pathway of Bulk mRNA Turnover. *Nat. Struct. Mol. Biol.* **2009**, *16*, 616–623.
4. Sement, F. M.; Ferrier, E.; Zuber, H.; Merret, R.; Alioua, M.; Deragon, J.-M.; Bousquet-Antonelli, C.; Lange, H.; Gagliardi, D. Uridylation Prevents 3′ Trimming of Oligoadenylated mRNAs. *Nucleic Acids Res.* **2013**, 1–13.
5. Malecki, M.; Viegas, S. C.; Carneiro, T.; Golik, P.; Dressaire, C.; Ferreira, M. G.; Arraiano, C. M. The Exoribonuclease Dis3L2 Defines a Novel Eukaryotic RNA Degradation Pathway. *EMBO J.* **2013**, *32*, 1–13.
6. Lubas, M.; Damgaard, C. K.; Tomecki, R.; Cysewski, D.; Jensen, T. H.; Dziembowski, A. Exonuclease hDIS3L2 Specifies an Exosome-Independent 3′-5′ Degradation Pathway of Human Cytoplasmic mRNA. *EMBO J.* **2013**, *32*, 1855–1868.
7. Heo, I.; Joo, C.; Kim, Y.-K.; Ha, M.; Yoon, M.-J.; Cho, J.; Yeom, K.-H.; Han, J.; Kim, V. N. TUT4 in Concert with Lin28 Suppresses MicroRNA Biogenesis through Pre-microRNA Uridylation. *Cell* **2009**, *138*, 696–708.
8. Jones, M. R.; Blahna, M. T.; Kozlowski, E.; Matsuura, K. Y.; Ferrari, J. D.; Morris, S. A.; Powers, J. T.; Daley, G. Q.; Quinton, L. J.; Mizgerd, J. P. Zcchc11 Uridylates Mature miRNAs To Enhance Neonatal IGF-1 Expression, Growth, and Survival. *PLoS Genet.* **2012**, *8*, e1003105–e1003115.
9. Burroughs, A M.; Kawano, M.; Ando, Y.; Daub, C. O.; Hayashizaki, Y. Pre-miRNA Profiles Obtained through Application of Locked Nucleic Acids and Deep Sequencing Reveals Complex 5′/3′ Arm Variation Including Concomitant Cleavage and Polyuridylation Patterns. *Nucleic Acids Res.* **2012**, *40*, 1424–1437.
10. Kasianowicz, J. J.; Brandin, E.; Branton, D.; Deamer, D. W. Characterization of Individual Polynucleotide Molecules Using a Membrane Channel. *Proc. Natl. Acad. Sci. U.S.A.* **1996**, *93*, 13770–13773.
11. Vercoutere, W.; Winters-Hilt, S.; Olsen, H.; Deamer, D.; Haussler, D.; Akeson, M. Rapid Discrimination Among Individual DNA Hairpin Molecules at Single-Nucleotide Resolution Using an Ion Channel. *Nat. Biotechnol.* **2001**, *19*, 248–252.
12. Sauer-Budge, A.; Nyamwanda, J.; Lubensky, D.; Branton, D. Unzipping Kinetics of Double-Stranded DNA in a Nanopore. *Phys. Rev. Lett.* **2003**, *90*, 238101–238105.
13. Stoddart, D.; Maglia, G.; Mikhailova, E.; Heron, A. J.; Bayley, H. Multiple Base-Recognition Sites in a Biological Nanopore: Two Heads Are Better Than One. *Angew. Chem., Int. Ed.* **2010**, *49*, 556–559.
14. Wallace, E. V. B.; Stoddart, D.; Heron, A. J.; Mikhailova, E.; Maglia, G.; Donohoe, T. J.; Bayley, H. Identification of Epigenetic DNA Modifications with a Protein Nanopore. *Chem. Commun.* **2010**, *46*, 8195–8197.
15. Ayub, M.; Bayley, H. Individual RNA Base Recognition in Immobilized Oligonucleotides Using a Protein Nanopore. *Nano Lett.* **2012**, *12*, 5637–5643.
16. Clarke, J.; Wu, H. C.; Jayasinghe, L.; Patel, A. Continuous Base Identification for Single-Molecule Nanopore DNA Sequencing. *Nat. Nanotechnol.* **2009**, 265–270.
17. Howorka, S.; Cheley, S.; Bayley, H. Sequence-Specific Detection of Individual DNA Strands Using Engineered Nanopores. *Nat. Biotechnol.* **2001**, *19*, 636–639.

18. Iqbal, S. M.; Akin, D.; Bashir, R. Solid-State Nanopore Channels with DNA Selectivity. *Nat. Nanotechnol.* **2007**, *2*, 243–248.
19. Wanunu, M.; Dadosh, T.; Ray, V.; Jin, J.; McReynolds, L.; Drndić, M. Rapid Electronic Detection of Probe-Specific MicroRNAs Using Thin Nanopore Sensors. *Nat. Nanotechnol.* **2010**, *5*, 807–814.
20. Lin, J.; Fabian, M.; Sonenberg, N.; Meller, A. Nanopore Detachment Kinetics of Poly(A) Binding Proteins from RNA Molecules Reveals the Critical Role of C-Terminus Interactions. *Biophys. J.* **2012**, *102*, 1427–1434.
21. Akeson, M.; Branton, D.; Kasianowicz, J. J.; Brandin, E.; Deamer, D. W. Microsecond Time-Scale Discrimination Among Polycytidylic Acid, Polyadenylic Acid, and Polyuridylic Acid as Homopolymers or as Segments within Single RNA Molecules. *Biophys. J.* **1999**, *77*, 3227–3233.
22. Meller, A.; Nivon, L.; Branton, D. Voltage-Driven DNA Translocations through a Nanopore. *Phys. Rev. Lett.* **2001**, *86*, 3435–3438.
23. Venkatesan, B. M.; Bashir, R. Nanopore Sensors for Nucleic Acid Analysis. *Nat. Nanotechnol.* **2011**, *6*, 615–624.
24. Rodriguez-Larrea, D.; Bayley, H. Multistep Protein Unfolding during Nanopore Translocation. *Nat. Nanotechnol.* **2013**, *8*, 288–295.
25. Chen, H.; Meisburger, S. P.; Pabit, S. A.; Sutton, J. L.; Webb, W. W.; Pollack, L. Ionic Strength-Dependent Persistence Lengths of Single-Stranded RNA and DNA. *Proc. Natl. Acad. Sci. U.S.A.* **2012**, *109*, 799–804.
26. Herrero-Galán, E.; Fuentes-Perez, M. E.; Carrasco, C.; Valpuesta, J. M.; Carrascosa, J. L.; Moreno-Herrero, F.; Arias-Gonzalez, J. R.; José, M.; Arias, J. R.; Page, S. Mechanical Identities of RNA and DNA Double Helices Unveiled at the Single-Molecule Level. *J. Am. Chem. Soc.* **2013**, *135*, 122–131.
27. Stoddart, D.; Heron, A. J.; Mikhailova, E.; Maglia, G.; Bayley, H. Single-Nucleotide Discrimination in Immobilized DNA Oligonucleotides with a Biological Nanopore. *Proc. Natl. Acad. Sci. U.S.A.* **2009**, *106*, 7702–7707.
28. Maglia, G.; Restrepo, M. R.; Mikhailova, E.; Bayley, H. Enhanced Translocation of Single DNA Molecules through Alpha-Hemolysin Nanopores by Manipulation of Internal Charge. *Proc. Natl. Acad. Sci. U.S.A.* **2008**, *105*, 19720–19725.
29. Wang, L.; Brown, S. J. BindN: A Web-Based Tool for Efficient Prediction of DNA and RNA Binding Sites in Amino Acid Sequences. *Nucleic Acids Res.* **2006**, *34*, 243–248.
30. DeGuzman, V. S.; Lee, C. C.; Deamer, D. W.; Vercoutere, W. A Sequence-Dependent Gating of an Ion Channel by DNA Hairpin Molecules. *Nucleic Acids Res.* **2006**, *34*, 6425–6437.
31. Achsel, T.; Brahms, H.; Kastner, B.; Bachi, A.; Wilm, M.; Lührmann, R. A Doughnut-Shaped Heteromer of Human Sm-like Proteins Binds to the 3′-End of U6 snRNA, Thereby Facilitating U4/U6 Duplex Formation *in Vitro*. *EMBO J.* **1999**, *18*, 5789–5802.
32. Törö, I.; Thore, S.; Mayer, C.; Basquin, J.; Séraphin, B.; Suck, D. RNA Binding in an Sm Core Domain: X-ray Structure and Functional Analysis of an Archaeal Sm Protein Complex. *EMBO J.* **2001**, *20*, 2293–2303.
33. Thore, S.; Mayer, C.; Sauter, C.; Weeks, S.; Suck, D. Crystal Structures of the *Pyrococcus abyssi* Sm Core and Its Complex with RNA. Common Features of RNA Binding in Archaea and Eukarya. *J. Biol. Chem.* **2003**, *278*, 1239–1247.
34. Fischer, S.; Benz, J.; Späth, B.; Maier, L.-K.; Straub, J.; Granzow, M.; Raabe, M.; Urlaub, H.; Hoffmann, J.; Brutschy, B.; *et al.* The Archaeal Lsm Protein Binds to Small RNAs. *J. Biol. Chem.* **2010**, *285*, 34429–34438.
35. Tang, W.; Kannan, R.; Blanchette, M.; Baumann, P. Telomerase RNA Biogenesis Involves Sequential Binding by Sm and Lsm Complexes. *Nature* **2012**, *484*, 260–264.
36. Gouaux, J. E.; Braha, O.; Hobaugh, M. R.; Song, L.; Cheley, S.; Shustak, C.; Bayley, H. Subunit Stoichiometry of Staphylococcal Alpha-Hemolysin in Crystals and on Membranes: A Heptameric Transmembrane Pore. *Proc. Natl. Acad. Sci. U.S.A.* **1994**, *91*, 12828–12831.
37. Hammerstein, A. F.; Jayasinghe, L.; Bayley, H. Subunit Dimers of Alpha-Hemolysin Expand the Engineering Toolbox for Protein Nanopores. *J. Biol. Chem.* **2011**, *286*, 14324–14334.
38. Cracknell, J. A.; Japrung, D.; Bayley, H. Translocating Kilobase RNA through the Staphylococcal α-Hemolysin Nanopore. *Nano Lett.* **2013**, *13*, 1–17.
39. van den Hout, M.; Vilfan, I. D.; Hage, S.; Dekker, N. H. Direct Force Measurements on Double-Stranded RNA in Solid-State Nanopores. *Nano Lett.* **2010**, *10*, 701–707.
40. Rissland, O. S.; Norbury, C. J. The Cid1 Poly(U) Polymerase. *Biochim. Biophys. Acta* **2008**, *1779*, 286–294.
41. Rissland, O. S.; Mikulasova, A.; Norbury, C. J. Efficient RNA Polyuridylation by Noncanonical Poly(A) Polymerases. *Mol. Cell. Biol.* **2007**, *27*, 3612–3624.
42. Carell, T.; Brandmayr, C.; Hienzsch, A.; Müller, M.; Pearson, D.; Reiter, V.; Thoma, I.; Thumbs, P.; Wagner, M. Structure and Function of Noncanonical Nucleobases. *Angew. Chem., Int. Ed.* **2012**, *51*, 7110–7131.
43. Maglia, G.; Heron, A. J.; Stoddart, D.; Japrung, D.; Bayley, H. Analysis of Single Nucleic Acid Molecules with Protein Nanopores. *Methods Enzymol.* **2010**, *475*, 591–623.
44. Oliphant, T. E. Python for Scientific Computing. *Comput. Sci. Eng.* **2007**, *9*, 10–20.
45. Behnel, S.; Bradshaw, R.; Citro, C.; Dalcin, L.; Seljebotn, D. S.; Smith, K. Python: An Ecosystem for Scientific Computing. *Comput. Sci. Eng.* **2011**, *13*, 31–39.
46. Garcia, S.; Davison, A.; Rodgers, C.; Yger, P.; Mahnoun, Y.; Estabanez, L.; Sobolev, A.; Brizzi, T.; Jaillet, F.; Rautenberg, P. *et al.*; http://neo.readthedocs.org (accessed June, 2013).